THE JOURNAL OF BIOLOGICAL CHEMISTRY
Vol. 277, No. 32, Issue of August 9, pp. 28459–28467, 2002
Printed in U.S.A.

Analysis of Nucleotide Binding to *Dictyostelium* Myosin II Motor Domains Containing a Single Tryptophan Near the Active Site*

Received for publication, March 6, 2002, and in revised form, April 17, 2002
Published, JBC Papers in Press, April 23, 2002, DOI 10.1074/jbc.M202180200

Mihály Kovács‡§¶, András Málnási-Csizmadia‡§, Robert J. Woolley‡, and Clive R. Bagshaw‡‖

From the ‡Department of Biochemistry, University of Leicester, Leicester LE1 7RH, United Kingdom and the §Department of Biochemistry, Eötvös Loránd University, Pázmány Péter Sétány 1/C, H-1117 Budapest, Hungary

Dictyostelium **myosin II motor domain constructs containing a single tryptophan residue near the active sites were prepared in order to characterize the process of nucleotide binding. Tryptophan was introduced at positions 113 and 131, which correspond to those naturally present in vertebrate skeletal muscle myosin, as well as position 129 that is also close to the adenine binding site. Nucleotide (ATP and ADP) binding was accompanied by a large quench in protein fluorescence in the case of the tryptophans at 129 and 131 but a small enhancement for that at 113. None of these residues was sensitive to the subsequent open-closed transition that is coupled to hydrolysis (*i.e.* ADP and ATP induced similar fluorescence changes). The kinetics of the fluorescence change with the F129W mutant revealed at least a three-step nucleotide binding mechanism, together with formation of a weakly competitive off-line intermediate that may represent a nonproductive mode of nucleotide binding. Overall, we conclude that the local and global conformational changes in myosin IIs induced by nucleotide binding are similar in myosins from different species, but the sign and magnitude of the tryptophan fluorescence changes reflect nonconserved residues in the immediate vicinity of each tryptophan. The nucleotide binding process is at least three-step, involving conformational changes that are quite distinct from the open-closed transition sensed by the tryptophan Trp^{501} in the relay loop.**

Interaction of nucleotides with vertebrate skeletal muscle myosin is accompanied by an enhancement in tryptophan fluorescence that has long been exploited to determine the mechanism of nucleotide binding and hydrolysis (1–3). Non-hydrolyzable nucleotides (*e.g.* ADP) cause a smaller enhancement than hydrolyzable ones (*e.g.* ATP), indicating that part of the fluorescence change observed with ATP may be associated with the hydrolysis step itself. The kinetics of binding saturate at high nucleotide concentrations, indicating that the process is at least two-step (1). Under some conditions, the fluorescence change associated with hydrolysis was resolved from a faster isomerization step (2). A more precise mechanism (Reaction 1) for the fluorescence enhancement associated with hydrolysis has recently been proposed using a *Dictyostelium discoideum* myosin construct containing a single tryptophan residue at position 501 in the relay loop, some 3 nm from the active site (4, 5).

We demonstrated that tryptophan at this position shows a small quench on nucleotide binding (10–20%) followed by a large enhancement (50–80%) associated with a major conformational change (4), presumably equivalent to the open-closed transition identified by x-ray crystallography (6). The latter step is freely reversible and slightly favors the open state (low fluorescence $M^{\dagger}$·ATP) in the presence of ATP under ambient conditions, but coupling to the hydrolysis step pulls the equilibrium over to the more stable M*ADP·P_i state with enhanced fluorescence (5). Thus, under most conditions, the kinetics of Trp^{501} enhancement upon interaction with ATP provide a measure of the hydrolysis reaction, in line with earlier schemes (2), although relaxation methods reveal these processes to be distinct events (5, 7). The quench in Trp^{501} fluorescence that precedes the enhancement is related to the binding process, but details of this step are not easy to characterize because the signal is small and is obscured by the subsequent open-closed transition. In the present study, we have made constructs containing single tryptophan residues near the active site with the aim of probing the initial binding step(s) without any contribution from the conformational changes that are coupled to hydrolysis.

The *D. discoideum* motor domain lacks tryptophan residues near the nucleotide site equivalent to positions Trp^{113} and Trp^{131} in vertebrate skeletal myosin. This finding has led to the suggestion that the enhancement seen upon ADP binding to vertebrate skeletal myosin may arise from specific perturbation of the tryptophan residues near the active site (6, 8). In skeletal muscle myosin, Trp^{131} lies in the vicinity of the adenine ring of the bound nucleotide, whereas the Trp^{113} side chain could be sensitive to nucleotide binding via interaction with the conservative Lys^{130} residue. We therefore have explored this idea by making the appropriate single tryptophan constructs in the *D. discoideum* motor domain. We previously showed that substitution of all of the naturally occurring tryptophan residues with phenylalanine in the *D. discoideum* motor domain had a fairly limited effect on the kinetic pathway (4), and hence adding back a single tryptophan residue as a site-directed probe at locations throughout the molecule is a potentially viable approach.

We found that tryptophan at position 113 in a *D. discoideum* construct does indeed respond with a small enhancement (3–5%) upon nucleotide binding; however, the residue at 131 gives a large (30%) quench, so overall the enhancement observed with vertebrate skeletal myosin cannot be accounted by simple analogy with the *D. discoideum* model constructs. Nevertheless, the large quench associated with Trp^{131} and of another construct, Trp^{129}, provided valuable signals to characterize the nucleotide binding steps that were otherwise unob-

* This work was supported by the BBSRC, Wellcome Trust, and the Magyary Zoltán Fellowship. The costs of publication of this article were defrayed in part by the payment of page charges. This article must therefore be hereby marked "*advertisement*" in accordance with 18 U.S.C. Section 1734 solely to indicate this fact.
¶ Supported by EMBO and the Hungarian Eötvös State Fellowship.
‖ To whom correspondence should be addressed. Tel.: 44-116-252-3454; Fax: 44-116-252-3369; E-mail: crb5@le.ac.uk.

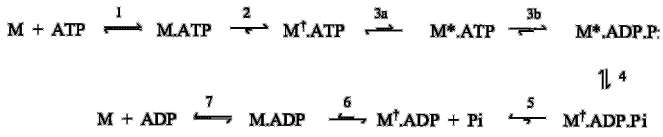

REACTION 1

servable in the wild-type *D. discoideum* motor domain (8, 9). These studies showed the nucleotide binding process is at least three-step, involving conformational changes that are quite distinct from the open-closed transition. Part of this work has previously been reported (10).

EXPERIMENTAL PROCEDURES

Nucleotides—ATP (special quality, vanadate-free) was from Roche Molecular Biochemicals. Other nucleotides were purchased from Sigma. The M·ADP·BeF_x complex (where BeF_x represents beryllium fluoride with undefined stoichiometry) was prepared by incubation of 5–20 μM motor domain, 50 μM ADP, 3 mM NaF, 50 μM $BeCl_2$ for 30 min. The M·ADP·AlF_4 complex was made similarly but with 50 μM $AlCl_3$ and incubation for at least 2 h. Mant-ATP[1] was purchased from Molecular Probes, Inc. (Eugene, OR).

Protein Engineering and Preparation—The constructs used in this study were based on the *D. discoideum* M761 motor domain (8) and thus have a modified N terminus, MDGTEDP . . . in place of MNP . . . , and a His-tagged C terminus . . . RLGSTRDALH$_8$, where Arg^{761} is the last native residue in the wild type sequence. DNA constructs containing the coding sequence for the W− (W36F, W432F, W501F, and W584F) and W501+ (W36F, W432F, and W584F) mutants of the M761 *D. discoideum* myosin II motor domain cloned into the pDXA-3H expression vector (11) were constructed as described earlier (4). Plasmids for the W113+ (W36F, W432F, W501F, W584F, and D113W), W129+ (W36F, W432F, W501F, W584F, and F129W), and W131+ (W36F, W432F, W501F, W584F, and R131W) mutants were produced from the pDXA/W− construct using PCR-based mutagenesis by introducing the mutations D113W, F129W, and R131W, respectively. The upstream primer used was 5′-ATGGATGGTACCGAGGATCCAATTCATG-3′, whereas we used 5′-GATTGGAATTCTCTTGAATGGATTGACGGCAACCAAAAAGAGACCTGAATAGGTGTAAATTAACCATTGATTGTAAGCAACACGG-3′ for D113W, 5′-TGGAATTCTCTTCCATGGATTGACGGCAACC-3′ for F129W, and 5′-ATCAACCATCTCTTGAGTGTAGATTGGAATCCACTTGAATGGATTGACGGC-3′ for R131W as the mutagenizing primer. A similar mutagenesis procedure was performed as in the case of W129+ to get the W129+/W501+ (W36F, W432F, W584F, F129W) DNA construct using pDXA/W501+ as the initial plasmid. All constructs were verified by DNA sequencing. Transformed *D. discoideum* cells were cultured, and the recombinant proteins were prepared as described previously (4). Protein concentrations were determined using Bradford reagent (Sigma). Purity of the preparations was checked by 9% SDS-PAGE.

ATPase Measurements—Steady-state basal MgATPase activities were measured from A_{340} using a pyruvate kinase-lactate dehydrogenase linked assay (12). Buffer conditions were 20 mM TES, 40 mM NaCl, 2 mM $MgCl_2$, pH 7.5. Assays were performed at 20 °C in the presence of 1 mM ATP, 200 μM NADH, 400 μM P-enolpyruvate, 10 units/ml pyruvate kinase, and 20 units/ml lactate dehydrogenase (P-0294; Sigma). MgATPase activities were measured on three different preparations in all cases.

Steady-state Fluorescence Measurements—Steady-state fluorescence spectra were measured with an SLM 48000 spectrofluorimeter (SLM Instruments, Urbana, IL) with a 200-watt mercury-xenon lamp or a 450-watt xenon lamp using a 5-mm path length cell (101.034-QS; Hellma, Westcliff-on-Sea, UK). Tryptophan was excited at 297 nm with 1-nm bandwidth to minimize photobleaching and to reduce inner filter effects at high nucleotide concentrations as well as to minimize contributions from tyrosine fluorescence emission. It was confirmed by control experiments that the added nucleotides did not have a significant inner filter effect at 297-nm excitation at concentrations used. Care was taken that ATP was not exhausted during recording the emission spectra.

Steady-state anisotropies were measured using the L format method with Glan-Thomson calcite prism polarizers. Tryptophan was excited at 297 nm with a 450-watt xenon lamp with 1-nm bandwidth. The vertical (parallel) and horizontal (perpendicular) emission components were detected successively through WG320 and UG11 filters (Comar Instruments, Cambridge, UK). The *G* factor was calculated from the ratio of intensities (I_v/I_h) when the excitation light was horizontally polarized. The *G* factor value was close to 1. The anisotropy values (*A*) were calculated from the intensity values of the vertical and horizontal measurements with correction for the detector *G* value ($A = (I_v - G{\cdot}I_h)/(I_v + 2{\cdot}G{\cdot}I_h)$).

Quantum yields were calculated using the comparative method, taking the value for free tryptophan of 0.13 (13). Fluorescence emission spectra of the proteins and tryptophan were recorded under "magic angle" polarizer conditions (*i.e.* excitation was vertical, and emission was 54° from vertical) and corrected using the calibration protocol supplied by SLM Instruments. Absorption spectra were recorded on a Pye Unicam SP8-100 spectrophotometer.

Acrylamide quenching experiments were performed as follows. Tryptophan was excited at 295 nm with 1-nm bandwidth, and the emission was detected using WG320 and UG11 filters. Samples of different acrylamide concentrations were measured immediately after mixing to avoid contributions from a slow fluorescence change. Data were fitted to the Stern-Volmer equation: $F_0/F = 1 + K_{SV}$[acrylamide], where F_0 and F are the fluorescence intensities in the absence and presence of the quencher, respectively, and K_{SV} is the dynamic quenching constant (13).

Transient Fluorescence Measurements—Transient fluorescence measurements were carried out using an Applied Photophysics SX18MV stopped-flow fluorimeter with a 150-watt xenon light source with excitation at 295 nm (2–4 nm bandwidth) with WG320 or WG335 cut-off emission filters in combination with a UG11 filter to block visible stray light. The instrument was modified to accept alternate sample cells to achieve a reduced dead time. The dead time of the apparatus with the 5-μl and 20-μl cell was 0.5 and 1.5 ms, respectively, as determined by the reaction of *N*-acetyl L-tryptophanamide with *N*-bromosuccinimide (14). These data are in good agreement with the Applied Photophysics SX18MV specifications. The signal level obtained was only 40% less with the 5-μl flow cell compared with the 20-μl cell, and thus, considering the 3-fold reduction in dead time, the smaller cell provided better resolution of fast (>500 s^{-1}) processes. ADP dissociation from the motor domain constructs was followed by rapid mixing with excess mant-ATP and monitoring mant fluorescence (excited at 356 nm) through a WG420 filter. Samples containing 2 μM protein and 50 μM ADP were mixed with mant-ATP solutions at varying concentrations (50–100 μM) to ensure that ADP dissociation was rate-limiting. All measurements were performed under buffer conditions 40 mM NaCl, 20 mM TES, 1 mM $MgCl_2$ at pH 7.5 in a thermostated cell. The reagent concentrations stated are reaction chamber concentrations. Data were collected on a logarithmic time base to ensure that there were a significant number of data points for all phases of multistep reactions (15). The ram profile of the instrument was checked by monitoring its position using the in-built linear potentiometer. Reaction profiles were analyzed by fitting to exponential functions using Origin, version 6.0 (Microcal Software). Reaction pathways were simulated using KinTekSim software (KinTek Corp.; www.kintek-corp.com/).

Time-resolved Fluorescence Measurements—Time-resolved fluorescence measurements were carried out using the time-correlated single photon counting method at the Rutherford Appleton Laboratory, Central Laser Facility (Didcot, UK). Fluorescence intensity and anisotropy decay profiles of the W129+ motor domain (9 μM samples) were recorded, and data were processed as described earlier for the W501+ mutant (16).

RESULTS

Protein Design, Expression, and ATPase Activity—In the present study, we examined four mutants of the *D. discoideum* myosin II motor domain comprising the first 761 amino acids of the protein. Truncation at this point does not alter the enzymic properties of *D. discoideum* myosin as was shown in earlier studies (8, 9). In the W113+, W129+, and W131+ single tryptophan mutants, all four tryptophans of the wild type motor domain were mutagenized to phenylalanine, and tryptophan residues were introduced in place of Asp^{113}, Phe^{129}, and Arg^{131}, respectively. Asp^{113} and Arg^{131} are the homologous positions for Trp^{113} and Trp^{131} of skeletal muscle myosin, whereas mutating *D. discoideum* Phe^{129} (Tyr^{129} in skeletal myosin) to

[1] The abbreviations used are: mant-, 2′(3′)-*O*-(*N*-methylanthraniloyl)-; AMP-PNP, adenosine 5′-(β,γ-imidotriphosphate); ATPγS, adenosine 5′-*O*-(3-thiotriphosphate); TES, *N*-tris(hydroxymethyl)-methyl-2-aminoethanesulfonic acid.

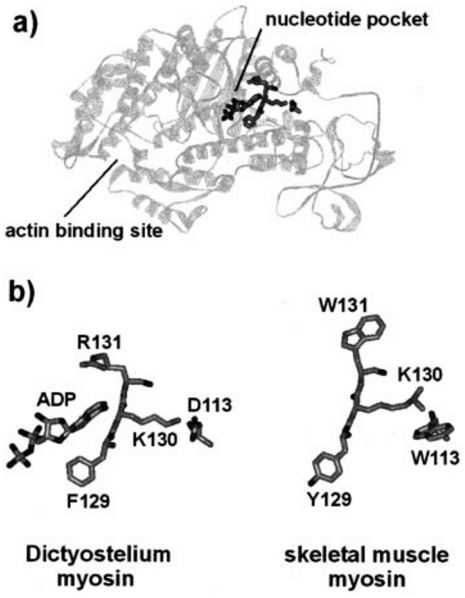

FIG. 1. *a*, location of residues 113 and 129–131 in the structure of the *D. discoideum* myosin II motor domain complexed with MgADP (18). *b*, the relative positions of these residues to the bound nucleotide in the *D. discoideum* myosin structure. The orientation of the corresponding residues of chicken skeletal muscle myosin (17) is shown for comparison.

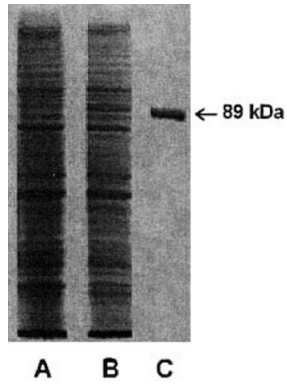

FIG. 2. **SDS-PAGE (9%) analysis of the purified recombinant protein.** *Lane A*, total lysate of the untransformed *D. discoideum* orf$^+$ cell line (10^5 cells). *Lane B*, total lysate of the same amount of cells expressing the W129+ motor domain. *Lane C*, affinity-purified protein preparation from the cell culture shown in *lane B*.

tryptophan represents a conservative substitution in close proximity to the adenine moiety of the bound nucleotide (17, 18) (Fig. 1, *a* and *b*). The latter position is occupied by an aromatic residue in almost all myosin classes sequenced to date (19). Thus, with these mutants the spectroscopic changes coming from Trp^{113} or Trp^{131} of skeletal muscle myosin might be mimicked in the absence of the background signal arising from the other tryptophans. The W129+/W501+ (W36F, W432F, W584F, and F129W) double tryptophan mutant also contains the conservative Trp^{501} residue (Trp^{510} in skeletal myosin, Trp^{512} in smooth muscle myosin) that has been identified as the residue responsible for the fluorescence enhancement concomitant with the open-closed conformational transition coupled to the hydrolysis step (4, 5, 20–23).

All mutants showed high levels of expression, and ~4 mg of recombinant protein could be prepared per liter of *D. discoideum* culture, whereas in the case of W129+ the yield was around 15 mg/liter. With the highly efficient affinity purification procedure, protein preparations of >99% purity could be obtained as shown in Fig. 2. Within experimental accuracy, the basal steady-state MgATPase activity of W129+/W501+ was the same as that of the wild type *D. discoideum* motor domain ($0.047 \pm 0.06\ s^{-1}$). In the case of W129+ and W131+, the rate was slightly altered by the mutations introduced ($0.036 \pm 0.04\ s^{-1}$ and $0.080 \pm 0.10\ s^{-1}$, respectively). W113+ yielded a rate of $0.05\ s^{-1}$ (single measurement). These findings are in line with previously reported observations that mutating the Trp^{501} residue to phenylalanine at most only moderately affects the ATPase rate (4), whereas in the W501Y-2R construct containing an artificial lever arm, the basal ATPase was not altered (20).

Steady-state Fluorescent Properties—Fig. 3*a* shows the uncorrected fluorescence emission spectra of the W113+, W129+, and W131+ mutants in the absence of nucleotide and in the presence of ADP. The excitation wavelength was 297 nm with narrow slits (1-nm bandwidth) to obtain maximal intensity changes on adding nucleotide. Both W129+ and W131+ responded with a large quench in fluorescence (55 and 30%, respectively) on ADP binding that was accompanied by a 7-nm blue shift in both cases. ADP binding to W113+ caused a small (3%) fluorescence increase and a 2-nm red shift in the emission. Adding ATP or nucleotide analogs to these constructs had the same effect on the emission spectra, which implies that none of these side chains are sensitive to the open-closed transition that follows step 2 (Reaction 1). The increase in intensity when ATP was added to W113+ was slightly higher than that for ADP (~5%, data not shown), but the difference between the signal of the ADP-bound state and the predominant component during steady-state ATPase was not large enough to clearly distinguish the different nucleotide-bound states. Interestingly, the binding of pyrophosphate to the W129+ motor domain causes a large increase (60%) and a 3-nm red shift in the fluorescence signal (Fig. 3*b*). As shown by crystallographic studies (24), pyrophosphate binds into the β- and γ-phosphate sites of the myosin active site. These data suggest that the decrease in W129+ fluorescence on binding of nucleotide may have a contribution from a direct quenching effect of the adenine moiety.

The addition of ATP to the W129+/W501+ construct caused a 50% increase in fluorescence and a 6-nm blue shift of the spectrum during the steady-state reaction, whereas a 30% quench and a smaller blue shift was seen on ADP binding (data not shown). These data, together with the finding that the I_{W129}/I_{W501} signal intensity ratio in the apo state is 0.56, are consistent with the 55% quench of W129+ emission upon nucleotide binding and a +80 to +100% and −17% signal change seen in W501+ upon adding ATP and ADP, respectively (4). The additivity of these signals might be expected because these side chains are 3 nm apart in the *D. discoideum* motor domain crystal structures (18) and thus unlikely to interact through efficient energy transfer (Förster distance = 0.9–1.8 nm) (13).

Dynamics of the Components of the W129+ Fluorescence Emission—The good protein yield of the W129+ construct, the large fluorescence change upon nucleotide addition, and its insensitivity to other events (*i.e.* open-closed transition) make it the most suitable mutant for analysis of the nucleotide binding site; therefore, we carried out more extensive measurements on this construct. Acrylamide quenching and time-resolved fluorescence measurements were performed to assess the origin of the signal changes. Upon the addition of nucleotide, K_{SV} drops to approximately half of the original value (Table I), which indicates that the Trp^{129} side chain is more shielded from the solvent when ATP or ADP is bound in the active site. The decrease in the W129+ fluorescence quantum yield upon nucleotide binding largely reflects the quench in fluorescence emission intensity (Table I), since its absorbance does not change significantly.

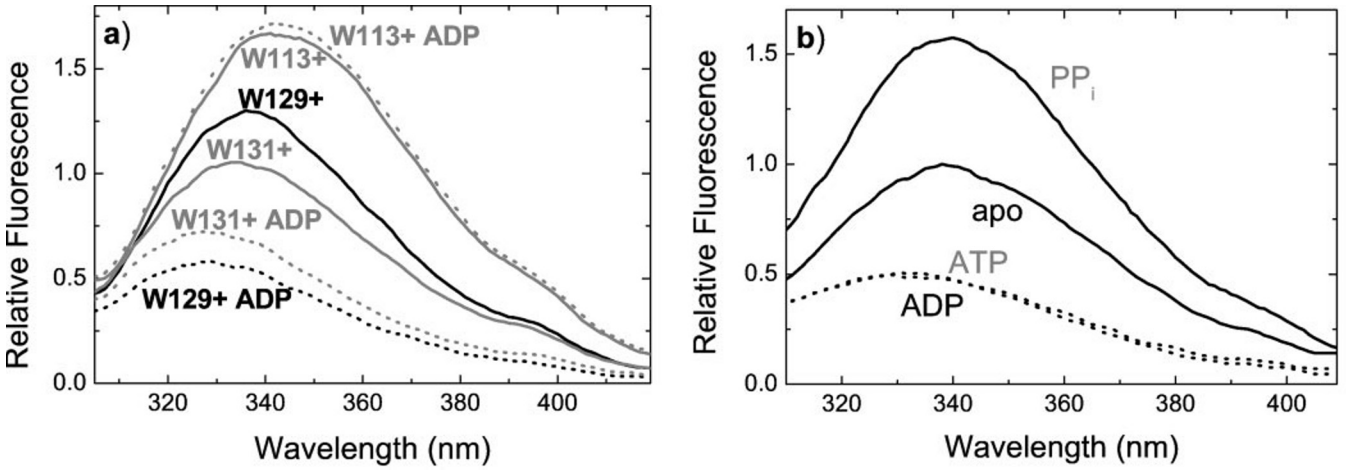

FIG. 3. *a*, uncorrected fluorescence emission spectra of the single tryptophan mutants W113+, W129+, and W131+ in nucleotide-free (*solid line*) and ADP-bound (*dashed line*) states. *b*, emission spectra of the W129+ motor domain in the absence of nucleotide and in ATP, ADP, and magnesium pyrophosphate. Spectra of 10 μM protein samples in 20 mM TES, 40 mM NaCl, 1 mM $MgCl_2$ at pH 7.5 were recorded at 20 °C (excitation wavelength was 297 nm, with 1-nm band widths). Added ligand concentrations were 1 mM ATP, 200 μM ADP, or 1 mM PP_i.

TABLE I
Steady-state and time-resolved fluorescence data of W129+ and W131+

	W129+			W131+		
	apo	ATP	ADP	Apo	ATP	ADP
Quantum yield	0.056	0.021	0.026	0.029	0.016	0.016
Steady state anisotropy	0.20	0.21	0.21	0.18	0.20	0.20
K_{sv} (acrylamide, M^{-1})	3.86	1.80	1.52			
t_1 (ns)	5.00	4.74	4.66			
t_2 (ns)	0.93	0.75	0.71			
Fluorescence lifetime components (%)						
Static	70	86	84			
t_1	16	6	7			
t_2	14	8	9			
Limiting anisotropy in time-resolved measurement	0.167	0.205	0.191			
Anisotropy decay time (ns)	120 ± 9	169 ± 24	118 ± 14			

Fluorescence intensity decay times were measured by time-resolved single photon counting. The decay profile was biphasic with ~1- and ~5-ns phases in all states (Fig. 4). Biphasic decay profiles with similar lifetime components have previously been observed with the W501+ single tryptophan construct (16). From these profiles and the observed quantum yields (assuming an intrinsic lifetime of 16 ns for free tryptophan), the proportion of the third, statically quenched component was calculated. Upon interaction with nucleotide, the proportion of the static component increases, and the relative proportion of the 5- and 1-ns components also changes from about 0.55–0.45 in apo to 0.45–0.55 in nucleotide-bound states (Table I). The amplitude of the decrease in the steady-state fluorescence intensity upon nucleotide addition can largely be accounted for by the increase in the proportion of the statically quenched tryptophan. This suggests that the quench could be due to the direct interaction of the indole moiety with the adenine ring, which is known to be a static quencher.

The high steady-state anisotropy of W129+ (about 0.2) shows that this side chain is rather immobile. In the nucleotide-bound states, slightly higher values were observed compared with the nucleotide-free state. Fluorescence anisotropy decay profiles were fitted to single exponentials to yield time constants above 100 ns (Table I). The values are in the time range of the rotational correlation time expected for the whole protein molecule and therefore indicate that the Trp^{129} side chain is immobile in all states. Similar measurements with W501+ gave decay times around 50 ns (16), suggesting that the emission dipole of the latter side chain is aligned along the short axis of the motor domain, whereas Trp^{129} is positioned along the long axis. Trp^{131} is also located close to the adenine moiety of the bound nucleotide and shows similar characteristics to Trp^{129} (*i.e.* the decrease in fluorescence quantum yield on ATP or ADP binding reflects mainly the change in emission intensity, and this side chain also has a high steady-state anisotropy with a further small increase on nucleotide binding) (Table I).

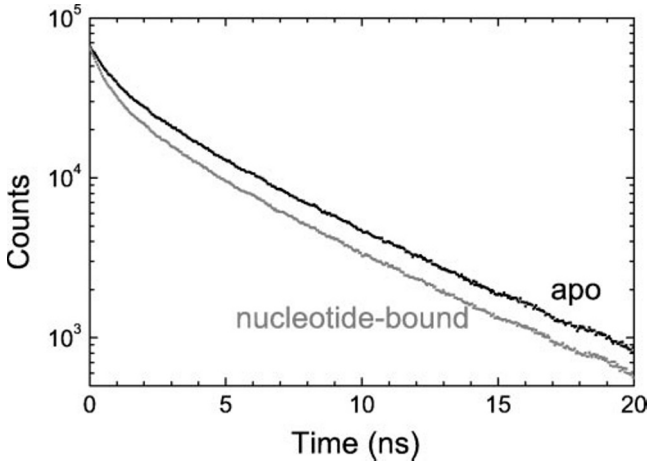

FIG. 4. **Intensity decay profile of the W129+ fluorescence emission measured by time-resolved single photon counting.** The decay was biphasic with ~1- and ~5-ns components in both the nucleotide-free and ADP-bound states. The decay profile in other nucleotide states (*i.e.* ATP, AMP-PNP, or ADP-AlF_4) was very similar to that observed with ADP (see also Table I).

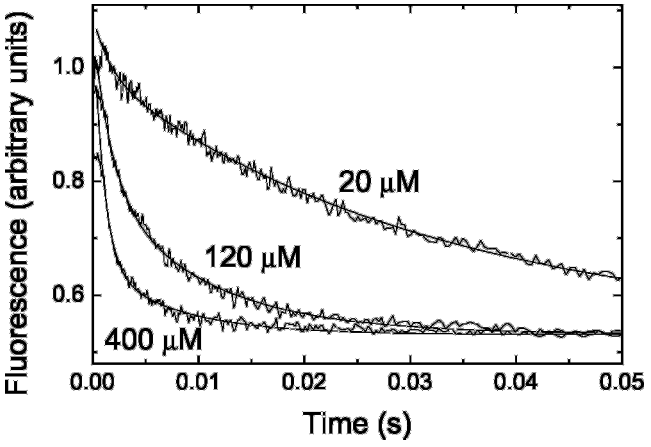

FIG. 5. **Sample traces of the reaction of W129+ (2 μM) with ADP at 20 °C.** Changes in tryptophan fluorescence (excited at 295 nm, 2-nm bandwidth) were monitored using WG320 and UG11 emission filters. Buffer conditions were as in Fig. 3. Records were captured on a logarithmic time base with the reactions starting at 0.4 ms pretrigger. The ram stopped at 0.9 ms. Traces were fitted to double exponentials. Observed rate constants were as follows: 1042 and 35 s^{-1} (20 μM), 637 and 110 s^{-1} (120 μM), 1053 and 147 s^{-1} (400 μM) (reaction chamber concentrations).

Transient Kinetics of Nucleotide Binding—The large signal changes due to the incorporation of an intrinsic fluorophore into the binding site allowed better resolution of the myosin nucleotide-binding transients than was possible in previous studies on skeletal muscle myosin. Also, to follow the very rapid processes in binding (around 1000 s^{-1}), we replaced the original 20-μl flow cell of the SX18MV stopped-flow apparatus with a 5-μl cell to obtain submillisecond dead time. The data were recorded on the same log time base throughout to avoid the effect of switching linear time bases on the weighting of the fits (15). Fig. 5 shows representative fluorescence stopped-flow traces of ADP binding to the W129+ motor domain. The observed quench is of similar amplitude to that seen in the emission spectra. When the curves were fitted to a single exponential, the observed rate constant showed saturation at high [ADP] with a maximum rate constant of about 1300 s^{-1} and an initial slope of 1.2×10^6 M^{-1} s^{-1}. However, the data at intermediate ADP concentrations (100–400 μM ADP) showed clear deviations from the fit, indicative of at least a biphasic process. The data were therefore analyzed using a double exponential, which gave a marked improvement in the residuals at intermediate [ADP], whereas the improvement in fit was marginal at the highest and lowest [ADP] used. A plot of the k_{obs} of the fast and slow phases against [ADP] yielded apparently distinct profiles (Fig. 6, *a* and *b*). The fast phase appeared to yield a large intercept value ($k_{obs} \approx 500$ s^{-1}), but its precise value was uncertain because at low [ADP] the amplitude was small. The slow phase had an intercept value of <5 s^{-1} in line with the expected dissociation rate constant (see below). At high [ADP], the fast and slow phases appeared to saturate at about 1000 s^{-1} and 150 s^{-1}, respectively, at 20 °C, but the amplitude of the slow phase was only about 20% of the total change (Fig. 6*c*). The high intercept value and shallow slope of the fast phase suggest the presence of a binding step with a low affinity ($K > 500$ μM). However, a simple in-line mechanism could not be found that would satisfy both a large intercept value and the apparent K_d of the slow phase of around 100 μM. Rather, two separate but competitive association processes were required. A number of schemes were modeled with this feature, including the Trybus-Taylor (3) mechanism with an extra weakly competitive nonproductive binding step to yield $M^{\#}$·ADP (Reaction 2). Overall, this side branch has little effect on the flux through the pathway, but it was sufficient to account for a positive intercept in the fast k_{obs}.

Simulations of Reaction 2 showed that the resultant profiles were triphasic, but only at intermediate [ADP] were three processes resolvable, and even then, the fit of a triphasic exponential was only a marginal improvement over a biphasic fit. When a simulated set of curves was analyzed by force fitting a biphasic exponential across the concentration range, a rate constant profile close to the experimental data could be generated (Fig. 6). The amplitude data also were reproduced by this scheme.

A second complication of the analysis arises from measuring rate constants in which a significant proportion of the reaction is lost in the dead time of the stopped-flow apparatus. The 5-μl cell has a dead time of 0.5 ms, and thus 40% of the amplitude of a reaction at 1000 s^{-1} is lost. The fluorescence profiles were analyzed in two ways to check the effect of the dead time losses. Either the origin of the curve was taken at the estimated time zero of the reaction and the amplitude was calculated from the fit at this time, or the fit was restricted to data points collected after the dead time. Either way, the resultant k_{obs} against [ADP] had similar profiles, but the actual values of the rate constants differed slightly. The fluorescence signal determined by extrapolation to zero time coincided with the fluorescence level determined by mixing the W129+ construct against buffer. Thus, these approaches were reasonably consistent and indicated that the loss in signal amplitude was more or less than expected on the basis of the resolved phases of the reaction and the known dead time. Thus, the total amplitude of the signal after correction for dead time was practically constant across the range of ADP concentrations above the overall K_d. When fitted to a biphasic curve, the corrected absolute amplitude of the fast phase increased from a 5 to 40% quench, and the slow phase decreased from a 45 to 5% quench with increasing [ADP]. At 100–200 μM [ADP], the contributions of the phases were roughly equal, but from the argument above, this apparent K_d is partly a reflection of fitting a biphasic curve to a triphasic profile. The same general results were found for the ADP binding profiles measured at 5 °C. The "fast phase" was not particularly temperature dependent, whereas k_{obs} of the slow phase decreased nearly 2-fold.

ATP binding to W129+ showed essentially similar profile to that of ADP. The amplitudes of the profiles were practically identical, indicating that there is little or no contribution of the open-closed transition or hydrolysis step to the signal from Trp^{129}. The maximum rate of the slow phase was 350 s^{-1} at 20 °C, and the intercept value of the fast phase was possibly slightly higher ($\leq$1100 s^{-1}) and saturated at 1800 s^{-1}.

Similar fluorescence profiles were obtained for the W131+ construct with ADP and ATP, but the overall amplitude was reduced to about 25% so that the extraction of phases was not as reliable. On the other hand, the enhancement seen for ADP and ATP binding to Trp^{113} was too small to yield reliable fits to multiphasic exponentials. A single exponential fit yielded similar rate constants to those observed when the W129+ and W131+ data were force-fit to a single exponential at low concentrations (apparent $k_{on} = 1.3 \times 10^6$ M^{-1} s^{-1}), whereas loss of amplitude at high [nucleotide] prevented an estimate of the maximum k_{obs}. We also note that the k_{obs} of ADP binding transients of the W501+ mutant also showed very similar concentration dependence, and there were indications that the binding process saturated with a rate constant > 250 s^{-1} (4). Thus, it is possible that the Trp^{501} side chain, which is located 3 nm from the binding site, is also sensitive to the events reported by Trp^{129} and Trp^{131}, but the fast and slow phases were unresolved because of the small total amplitude of the

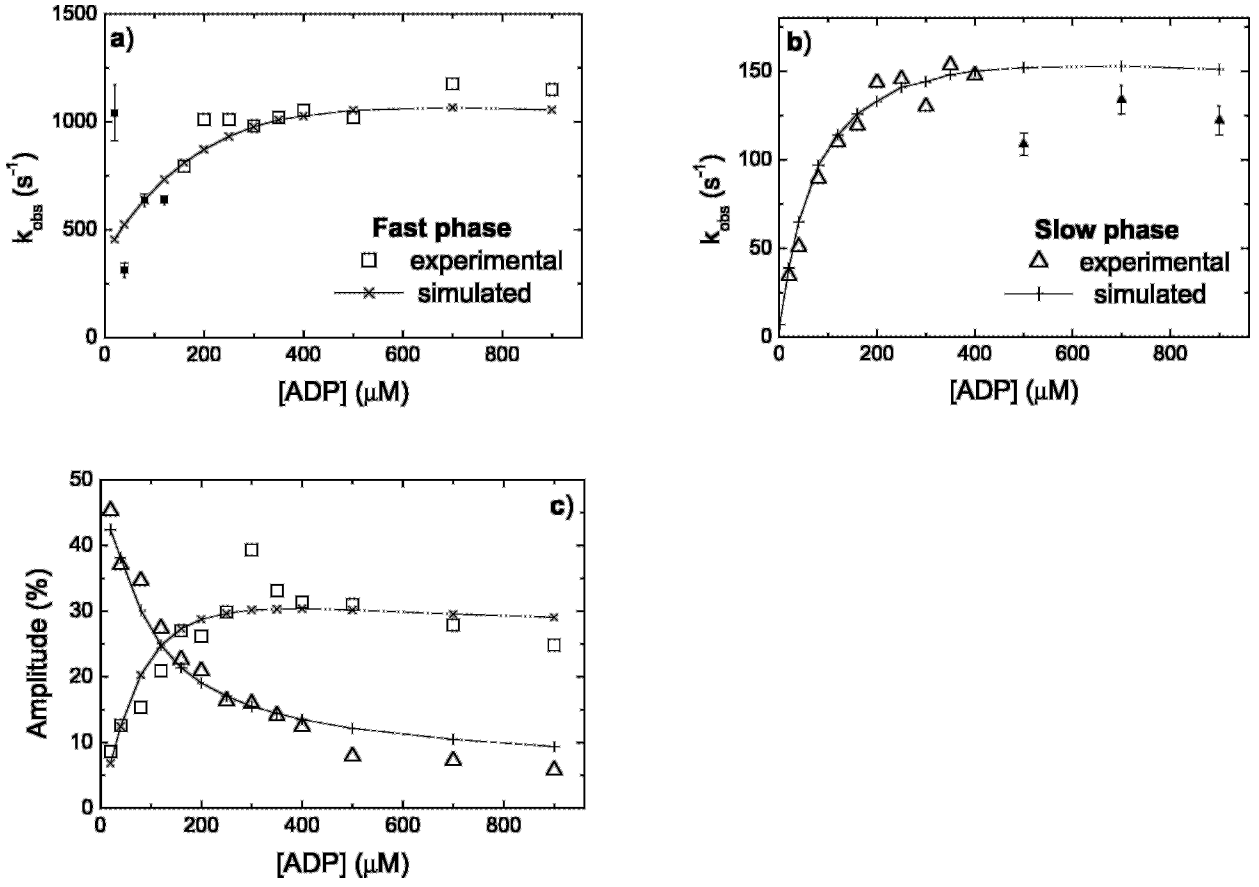

FIG. 6. **Rate and amplitude data from biphasic fits of the W129+ ADP binding transients (see Fig. 5), plotted against nucleotide concentration.** Traces could be fitted to double exponential functions without major systematic deviations throughout the whole concentration range studied. Rate constants for the fast and slow phases are shown in *a* and *b*, respectively. *Small solid symbols* indicate data points where the fit was less certain because the amplitude was small. *c*, amplitudes of the fast (*solid squares*) and slow (*open triangles*) phases, relative to the total signal level. The *solid lines* with *crosses* were obtained from a biphasic fit to simulated data for a three-step scheme (Reaction 2) in which $k_1 = 10$ $\mu M^{-1}\cdot s^{-1}$, $k_{-1} = 1300$ s^{-1}, $k_{2a} = 500$ s^{-1}, $k_{-2a} = 50$ s^{-1}, $k_{2b} = 140$ s^{-1}, $k_{-2b} = 10$ s^{-1}, with a competing branch step $k_{\#} = 2$ $\mu M^{-1}\cdot s^{-1}$, $k_{-\#} = 700$ s^{-1} (*i.e.* the overall K_d for ADP binding was about 1 μM). Simulation of the observed dissociation rate constant of ADP from the $M^{\dagger}_2\cdot ADP$ by displacement state gave $k_{obs} = 2$ s^{-1}, whereas the intercept value of the "slow" phase in the simulated data was 7 s^{-1}. It is apparent that the intercept value of the "fast" phase is dominated by $k_{-\#}$, whereas the maximum rate constant of the "fast" and "slow" phases have dominant contributions from k_{2a} and k_{2b}, respectively. However, these assignments are not precise because there are three rather than two phases present (see "Results"), and each phase has a significant contribution from several rate constants. The addition of a further step that allowed direct rearrangement of the M#·L species to M·L without dissociation and rebinding had a marginal effect on the transient profile. In the simulation shown, the quench of the $M^{\#}\cdot L$ species was twice that of the $M^{\dagger}_1\cdot L$ and $M^{\dagger}_2\cdot L$ species. This is the maximum quench that can be assigned to M#·L, since it corresponds to a total quench relative to the apo state (M).

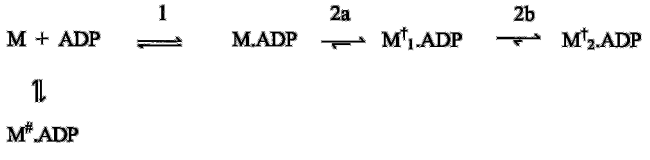

REACTION 2

fluorescence quench experienced by Trp^{501}.

The rate constants for ADP dissociation from W129+ and W131+ were determined by ADP displacement by excess mant-ATP as a chaser as 0.8 ± 0.1 s^{-1} (W129+) and 1.7 ± 0.3 s^{-1} (W131+). These values are consistent with the upper limits set by the *y* intercepts of the nucleotide concentration dependence of the slow phase rates extracted from the binding transients.

W129+ fluorescence enhancement on pyrophosphate binding is a much slower process than the quench seen on nucleotide addition. Fig. 7*a* shows a stopped-flow record of the reaction of W129+ (2 μM) with 100 μM PP_i. The traces were monophasic, and the observed rate constant showed hyperbolic dependence on [PP_i] (Fig. 7*b*). k_{obs} saturated at 0.58 ± 0.02 s^{-1}, reaching half-maximum at 89 ± 11 μM.

Upon rapid mixing with ATP, the W129+/W501+ double tryptophan mutant showed an initial large quench followed by a large enhancement (Fig. 8*a*). The rate of the fast quench phase plotted against [ATP] had an initial slope of 1.80 ± 0.02 × 10^6 M^{-1} s^{-1}, with an indication of saturation around 500 s^{-1} (Fig. 8*b*). The rate of the slow enhancement plateaued at 8 s^{-1} (Fig. 8*c*), which indicates that the hydrolysis step in this mutant is slower than in the wild-type (where this value is around 30 s^{-1}). The traces of the reaction with ADP fitted a monophasic exponential satisfactorily, and the dependence of k_{obs} on [ADP] had an initial slope of 0.42 ± 0.01 × 10^6 M^{-1} s^{-1} with a *y* intercept of 3.1 ± 0.2 s^{-1}, in agreement with the results of the ADP displacement experiment (not shown).

DISCUSSION

Despite the long history (1–3), the assignment of tryptophan fluorescence changes to specific steps in the vertebrate skeletal muscle myosin and actomyosin ATPase pathways has been controversial and difficult to resolve for a number of reasons. At 20 °C, the rapid isomerization steps are lost within the dead time of the stopped flow apparatus, and only the fluorescence change associated with hydrolysis is clearly resolved. At lower temperatures, additional steps were resolved, which suggested that there are at least two binding isomerizations that are

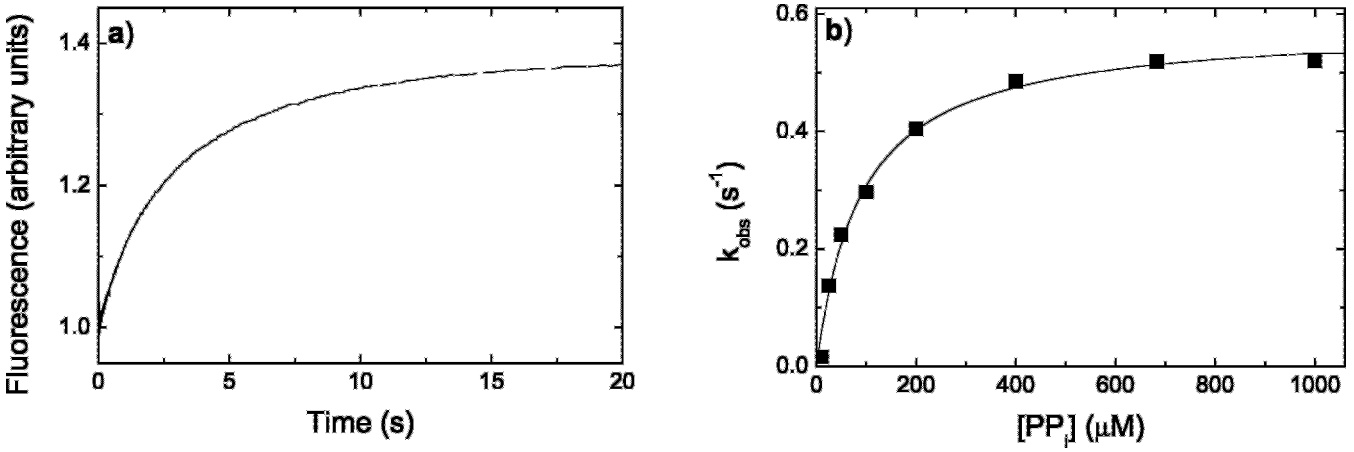

FIG. 7. *a*, stopped-flow record of the reaction of W129+ (2 μM) with 100 μM PP_i. *b*, the observed rate constants at different ligand concentrations (reaction chamber). Traces were fitted to single exponentials. k_{obs} had a hyperbolic dependence on [PP_i] with a maximum rate constant of 0.58 ± 0.02 s^{-1} (half-saturation at 89 ± 11 μM; initial slope: 5 ± 1 × 10^3 M^{-1} s^{-1}). Experiments were performed at 20 °C. Buffer conditions were as in Fig. 3.

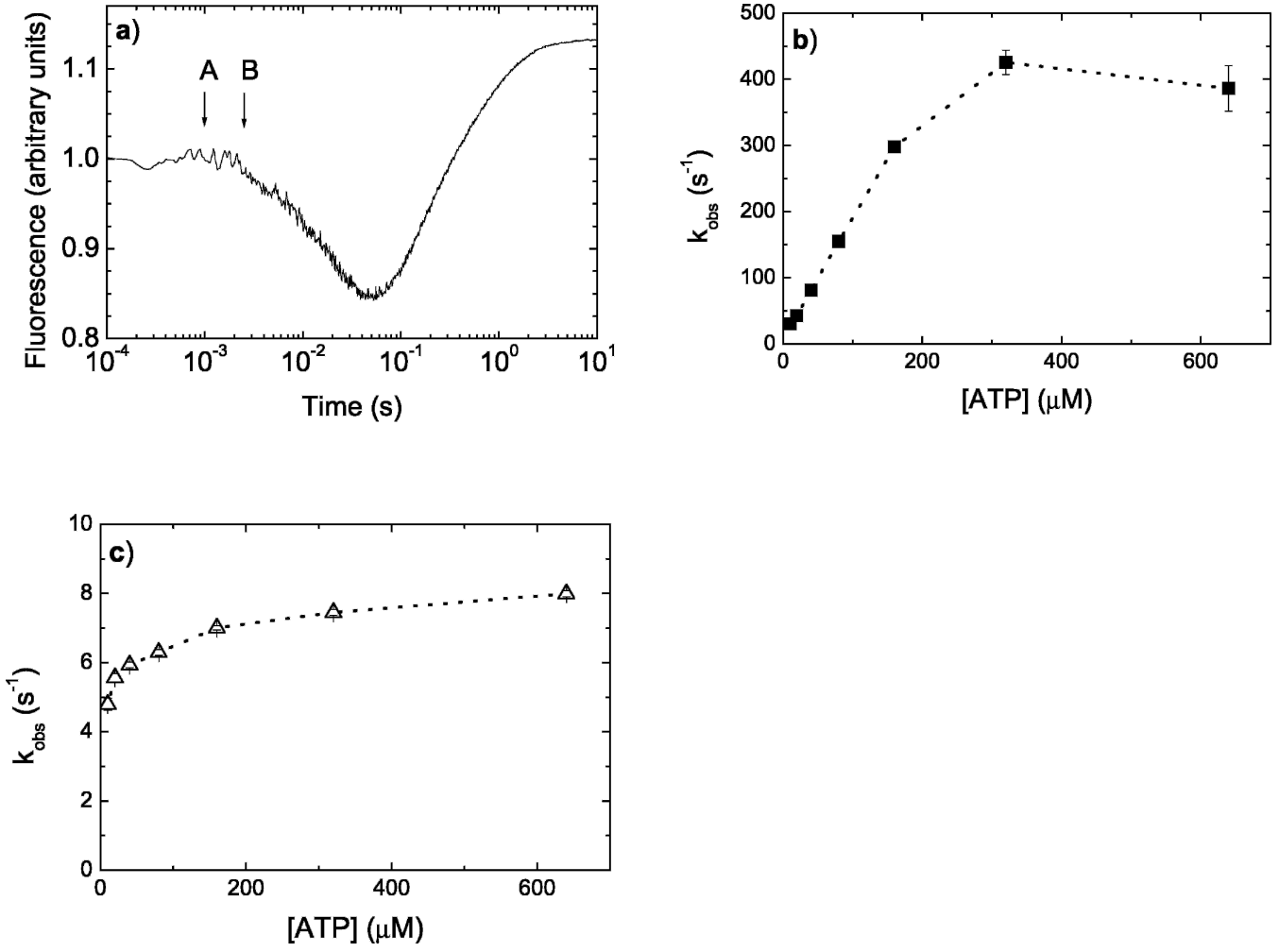

FIG. 8. *a*, stopped-flow record of the reaction of 2 μM W129+/W501+ with 20 μM ATP at 20 °C (reaction chamber concentrations). Tryptophan fluorescence (excited at 295 nm, 2-nm bandwidth) was monitored through WG320 and UG11 filters. Data are plotted on a logarithmic time base. *Arrow A* shows the calculated starting point of the reaction whereas the stop of the ram is marked by *arrow B*. *b* and *c*, dependences of the observed rate constants of the reaction of W129+/W501+ with ATP on nucleotide concentration. *b*, the k_{obs} of the fast quench phase was linearly dependent on [ATP] in the range of 0–160 μM (slope: 1.80 ± 0.02 × 10^6 M^{-1} s^{-1}). *c*, the rate of the slow enhancement phase reached a plateau of about 8 s^{-1}. Buffer conditions were as in Fig. 3.

distinct from the hydrolysis step (3). In the presence of actin, there are further complications arising from the potential of tryptophans in actin to contribute to the signal change, perturbations of myosin tryptophans that are sensitive to actin binding (2, 25), and the technical difficulty of the effect of light scattering changes on the measured fluorescence signal (26). Use of *D. discoideum* myosin II constructs has the advantage that tryptophan residues can be added or removed by mutagen-

esis to probe specific regions of the myosin motor domain. Here we focus on the response of tryptophan residues located near the myosin nucleotide binding site. We show that a tryptophan residue at position 129 or 131 responds with similar kinetics (after allowing for species differences) as previously characterized for rabbit skeletal myosin (3), although the fluorescence change is in the opposite direction. The cause of the fluorescence enhancement on nucleotide binding seen with vertebrate myosins has therefore not been unambiguously identified. There are several candidates for the source of the signal change in vertebrate myosins. First, the two tryptophans in the vicinity of the binding site (Trp^{113} and Trp^{131} in rabbit skeletal myosin), which are conserved only among skeletal and cardiac muscle isoforms, are likely to be sensitive to nucleotide binding (6, 8), although their local environments may be different from those in *D. discoideum* myosin to give a net enhancement rather than quench. Park and Burghardt (21) isolated Trp^{131} emission in skeletal muscle subfragment 1 by means of elimination of its fluorescence contribution using site-specific chemical modification. Their data show that this side chain indeed responds with a ~20% enhancement upon binding of nucleotide, but they excluded Trp^{131} as the tryptophan sensitive to ATP hydrolysis on the basis that the signal was similar in different nucleotide states. Based on structural data, Trp^{113} also cannot be excluded as a potential candidate responsible for nucleotide binding-induced signal changes. The contribution of these residues to the signal change is also indicated by the fact that wild-type *D. discoideum* myosin II, which lacks Trp^{131} (and Trp^{113}), does not respond with a significant change in fluorescence on nucleotide binding (8, 9). The single tryptophan residues of the *D. discoideum* myosin mutants presented in this study (Trp^{113}, Trp^{129}, and Trp^{131}) were insensitive to the events of the ATPase cycle other than nucleotide binding. However, the combined contributions of Trp^{113} and Trp^{131} would lead to a net quench rather than enhancement on nucleotide binding.

The conservative tryptophan residue in the relay loop of the motor domain (Trp^{510} in skeletal, Trp^{512} in smooth muscle, and Trp^{501} in *D. discoideum* myosin), which is sensitive to the open-closed transition, also shows a fluorescence change upon nucleotide binding. Skeletal and smooth muscle myosin relay loop tryptophans show 38 and 30% enhancement upon ADP addition, respectively (21, 22). In the W501+ single tryptophan *D. discoideum* myosin mutant, a 15–20% quench can be detected on this step (4, 5). It is unlikely that other tryptophans are involved (*e.g.* the conserved Trp^{432} in *D. discoideum*, Trp^{440} in skeletal myosin) because the W501F and W501Y mutants show almost no fluorescence change upon adding nucleotide (4, 20). Our data therefore indicate that (i) both the tryptophan(s) near the binding site and the relay loop residue contribute to the fluorescence change upon nucleotide binding prior to the open-closed transition, and (ii) the direction and extent of the fluorescence change of the responsive tryptophans is largely determined by the nonconservative environment surrounding the tryptophan side chain. Thus, we conclude that the global conformational changes undertaken by these myosins are conserved (on the basis of similar rate profiles and functional properties), and even the local movement of particular tryptophan residues could be similar, but the environment experienced by the tryptophan side chains during such movements will vary because of nonconserved residues around them.

The acrylamide quenching experiments indicate that a tryptophan residue at position 129 is solvent-exposed, as expected from the crystal structures (17, 18). Nevertheless, time-resolved anisotropy measurements indicate that this side chain is not freely mobile, and interconversion between rotamer states occurs on a time scale slower than net rotation of the motor domain, as was also noted for Trp^{501} (16). Nucleotide binding is accompanied by a protection of Trp^{129} from collisional quenching by agents in solution, but this residue is now subject to increased static quenching, possibly by direct association with the adenine moiety.

Regardless of the specific origin of the fluorescence change, the large quench observed on nucleotide binding to W129+ allows a more precise analysis of the mechanism than has hitherto been possible with wild-type proteins. Furthermore, the signal from Trp^{129} is not sensitive to the open-closed transition, which removes some of the ambiguity in the analysis. This is particularly important because much of the earlier data exploited analogs such as AMP-PNP and ATPγS to mimic the nonhydrolyzed ATP state, but it is now known that these analogs induce the closed state to a limited extent (4, 5, 7) and hence have a contribution from the signal traditionally assigned to the $M^{*}{\cdot}ADP{\cdot}P_i$ state ($M^{**}{\cdot}ADP{\cdot}P_i$ in skeletal myosin). ADP has less or no tendency to induce the closed state (5, 7) and is therefore the simplest nucleotide with which to explore the initial binding steps.

In accordance with this concept, the overall profiles of different nucleotides binding to the W129+ construct were similar in character to that observed by Trybus and Taylor (3) for ADP binding to skeletal myosin at 5 °C (at higher temperatures, the isomerization steps with skeletal myosin are too fast to resolve). The profiles of skeletal and *D. discoideum* myosins differ in detail in the near loss of the slow phase at high [nucleotide], which indicates that the $M^{\dagger}_1{\cdot}L$ and $M^{\dagger}_2{\cdot}L$ states have nearly the same fluorescence yield in *D. discoideum* myosin (hence at saturating [nucleotide], step 2b is optically silent). Furthermore, the k_{obs} of the fast phase appeared to extrapolate back to give a large intercept value (250–1000 s^{-1}), whereas it was close to zero in the Trybus and Taylor (3) data. This aspect is difficult to characterize with accuracy, However, it can be accounted for by an additional weak but competitive nonproductive binding mode of the nucleotide as in Reaction 2. Here, M#·L might represent a nucleotide bound to the active site in a noncompetent orientation that must dissociate and reassociate (or rearrange while bound) before forming the tightly bound form $M^{\dagger}_2{\cdot}L$.

The fluorescence transients from the double tryptophan construct, W129+/W501+, show a clear distinction between the nucleotide binding steps and the open-closed transition that is coupled to hydrolysis, because the signals have opposite signs (*cf.* skeletal myosin, where they both give enhancements). Furthermore, the effective hydrolysis rate is slowed to 8 s^{-1} at 20 °C, which may be useful for developing conformationally resolved single molecule ATPase assays because the transition occurs on the time scale appropriate for video acquisition (27).

Although the aim of this work was to characterize the tryptophan residue(s) in the motor domain that respond to the nucleotide binding steps and to exploit the fluorescence signal to delineate the elementary steps of this process, it is of interest to relate these steps to those that occur in the presence of actin. Previous studies have estimated that the ATP-induced dissociation of acto-*D. discoideum* motor domain is limited by a first order step of 150–450 s^{-1} at 20 °C (8, 9) and is thus comparable with the slower of the two isomerization steps revealed by Trp^{129} fluorescence. We confirm that the acto-W129+ construct dissociates with a maximum rate constant of 150 s^{-1} at saturating [ATP]. The conformational changes sensed by the tryptophan residues near the active site (Trp^{129} and Trp^{131}) are therefore likely to occur before or are coincident with the ATP-induced actomyosin dissociation reaction. This is in agreement with thermodynamic arguments that require coupling with an

effectively irreversible step (step 2b with ATP) in the binding mechanism to provide sufficient energy to drive the actomyosin dissociation reaction. We find no evidence of a slower tryptophan fluorescence change sensed by Trp^{129} after actin dissociation, but previous reports with skeletal myosin where this was observed may reflect a contribution from the open-closed transition (26). Single tryptophan-containing constructs will provide a valuable tool for further delineating communication pathways between the actin site, nucleotide site, and converter region of myosins.

Acknowledgments—We thank Dr. Stanley R. Botchway (Rutherford Appleton Laboratory) for assistance in conducting the time-correlated single photon counting measurements.

REFERENCES

1. Bagshaw, C. R., Eccleston, J. F., Eckstein, F., Goody, R. S., Gutfreund, H., and Trentham, D. R. (1974) *Biochem. J.* **141,** 351–364
2. Johnson, K. A., and Taylor, E. W. (1978) *Biochemistry* **17,** 3432–3442
3. Trybus, K. M., and Taylor, E. W. (1982) *Biochemistry* **21,** 1284–1294
4. Málnási-Csizmadia, A., Woolley, R. J., and Bagshaw, C. R. (2000) *Biochemistry* **39,** 16135–16146
5. Málnási-Csizmadia, A., Pearson, D. S., Kovács, M., Woolley, R. J., Geeves, M. A., and Bagshaw, C. R. (2001) *Biochemistry,* **40,** 12727–12737
6. Geeves, M. A., and Holmes, K. C. (1999) *Annu. Rev. Biochem.* **68,** 687–728
7. Urbanke, C., and Wray, J. (2001) *Biochem. J.* **358,** 165–173
8. Kurzawa, S., E., Manstein, D. J., and Geeves, M. A. (1997) *Biochemistry* **36,** 317–323
9. Kuhlman, P. A., and Bagshaw, C. R. (1998) *J. Muscle Res. Cell Motil.* **19,** 491–504
10. Kovács, M., Málnási-Csizmadia, A., Woolley, R. J., and Bagshaw, C. R. (2002) Biophys. J. **82,** 407 (abstr.)
11. Manstein, D. J., Schuster, H. P., Morandini, P., and Hunt, D. M. (1995) *Gene* (*Amst.*) **162,** 129–134
12. Trentham, D. R., Bardsley, R. G., Eccleston, J. F., and Weeds, A. G. (1972) *Biochem. J.* **126,** 635–644
13. Lakowicz, J. R. (1999) *Principles of Fluorescence Spectroscopy*, 2nd Ed., Kluwer Academic, New York
14. Peterman, B. F. (1979) *Anal. Biochem.* **93,** 442–444
15. Walmsley, A. R., and Bagshaw, C. R. (1989) *Anal. Biochem.* **176,** 313–318
16. Málnási-Csizmadia, A., Kovács, M., Woolley, R. J. Botchway, S. W., and Bagshaw, C. R. (2001) *J. Biol. Chem.* **276,** 19483–19490
17. Rayment, I., Rypniewski, W. R., Schmidt-Bäse, K., Smith, R., Tomchick, D. R., Benning, M. M., Winkelmann, D. A., Wesenberg, G., and Holden, H. M. (1993) *Science* **261,** 50–58
18. Gulick A. M., Bauer C. B., Thoden J. B., and Rayment, I. (1997) *Biochemistry* **36,** 11619–11628
19. Sellers, J. R. (1999) *Myosins* (2nd Ed.) Oxford University Press, Oxford
20. Batra, R., and Manstein, D. J. (1999) *Biol. Chem.* **380,** 1017–1023
21. Park, S., and Burghardt, T. P. (2000) *Biochemistry* **39,** 11732–11741
22. Yengo, C. M., Chrin, L. R., Rovner, A. S., and Berger, C. L. (2000) *J. Biol. Chem.* **275,** 25481–25487
23. Onishi H, Konishi, K., Fujiwara, K., Hayakawa, K., Tanokura, M., Martinez, H. M., and Morales, M. F. (2000) *Proc. Natl. Acad. Sci. U. S. A.* **97,** 11203–11208
24. Smith, C. A., and Rayment, I. (1995) *Biochemistry* **34,** 8973–8981
25. Yengo, C. M., Chrin, L., Rovner, A. S., and Berger, C. L. (1999) *Biochemistry* **38,** 14515–14523
26. Millar, N. C., and Geeves, M. A. (1988) *Biochem. J.* **249,** 735–743
27. Bagshaw C. R., and Conibear, P. B. (2000) *Single Mol.* **1,** 269–275